Available online at www.sciencedirect.com

SciVerse ScienceDirect

Ceramics International 39 (2013) 4391–4398

CERAMICS INTERNATIONAL

www.elsevier.com/locate/ceramint

Effect of niobium doping on opto-electronic properties of sol–gel based nanostructured indium tin oxide thin films

Saeed Mohammadi, Hossein Abdizadeh, Mohammad Reza Golobostanfard*

School of Metallurgy and Materials Engineering, College of Engineering, University of Tehran, P.O. Box 11155-4563, Tehran, Iran

Received 9 August 2012; received in revised form 31 October 2012; accepted 9 November 2012
Available online 19 November 2012

Abstract

Optically transparent conducting niobium-doped indium tin oxide (ITNO) thin films were deposited on soda lime glass via sol–gel spin coating technique under various Nb-doping contents. The effect of different Nb-dopant contents on the opto-electronic as well as microstructural properties of the films were characterized by means of UV–vis spectroscopy, four point probe, X-ray diffraction (XRD), field emission scanning electron microscopy (FESEM), and atomic force microscopy (AFM). For this purpose, addition of different Nb contents with tin at fixed 6 at% is considered as the first approach. For the second and third approaches, different Nb-doping contents were added at fixed atomic ratios of In:Sn=94:6 and In:Sn=95:5, respectively. Optimum opto-electronic properties, including minimum resistivity of $37.2\times10^{-3}\ \Omega$ cm with average transmittance of about 85% in the visible region and band gap of 3.48 eV was achieved for ITNO thin films prepared by the first approach at Nb and Sn doping content of 1 and 5 at%, respectively. XRD analysis revealed patterns of cubic bixbyite structure of In_2O_3 and rhombohedral structure of ITO for Nb-doped films with small shift in major peak position to lower diffraction angles with the addition of Nb. FESEM micrographs show that addition of Nb causes clustering of the grains at higher doping content. However, AFM studies show that addition of Nb dopant leads to the formation of films with compact surface and less average roughness compare to the undoped ITO films.

Keywords: Indium tin oxide; Nb doping; Sol–gel spin coating; Opto-electronic properties

1. Introduction

Transparent conductive oxides (TCOs) are widely used in a large variety of opto-electronic fields such as dye synthesized solar cells [1], liquid crystal displays [2,3], organic light emitting diodes [4], and gas sensing devices [5] because of their high electrical conductivity and good optical transparency in the visible regions. Some TCOs such as tin doped indium oxide (ITO), fluorine doped tin oxide (FTO), aluminum doped zinc oxide (AZO), and antimony doped tin oxide (ATO) are the most commonly used materials for opto-electronic applications. Among those, ITO has received particular attention due to its good transparency, high conductivity, and chemical stability [6–8]. However, in recent years, a variety of strategies has been considered to improve the electrical and optical properties of the In_2O_3-based materials [9] in order to achieve good compromise between electrical conductivity and transparency in the visible region. Based on literature, opto-electronic properties of TCOs are highly dependent on the nature and content of the added impurity rather than optimization of preparation parameters such as annealing temperature and thickness of the films [10]. In this communication, different types of impurities, including tin (Sn), gallium (Ga), copper (Cu), zirconium (Zr), zinc (Zn), titanium (Ti), tungsten (W), molybdenum (Mo), and niobium (Nb), have been doped into the In_2O_3-based matrix [11–22]. Recently, development of Nb-doped In_2O_3 (INO) thin films with high conductivity and transparency was reported by Gupta et al. [21,22]. Addition of Nb-dopant has many advantages including increase of electrical conductivity due to valence difference between Nb^{+5} ions and substituted In^{+3} ions, and low impurity scattering because of decrease in free carrier absorption in the near-infrared (NIR) region by adding low Nb-dopant

*Corresponding author. Tel.: +98 61114157; fax: +98 21 88006076.
E-mail address: Bostanfr@ut.ac.ir (M.R. Golobostanfard).

0272-8842/$ - see front matter © 2012 Elsevier Ltd and Techna Group S.r.l. All rights reserved.
http://dx.doi.org/10.1016/j.ceramint.2012.11.027

content. Recent researches on development of INO thin films have mainly focused on the effect of oxygen partial pressure [21] and substrate temperature [22] in the constant Nb-doping content via pulsed laser deposition technique as well as addition of different Nb-doping contents in In_2O_3 matrix in constant preparation process via magnetron sputtering method [23]. With regard to appropriate properties of Nb dopant in In_2O_3 lattice in terms of both the electrical resistivity and electron scattering and expensiveness of the Nb dopant, the aim of this work is devoted to investigate the behavior of Nb as a co-dopant beside Sn to improve the opto-electronic properties of the In_2O_3 films. In other words, it is worth investigating the addition of different Nb-doping contents in ITO thin films via sol–gel spin coating technique, in order to obtain new TCO with comparable opto-electronic properties with ITO thin films.

2. Experimental procedures

2.1. Sol preparation

The indium tin niobium oxide (ITNO) sol was prepared from anhydrous $InCl_3$ (Alfa Aesar, 99.99%), $SnCl_2 \cdot 2H_2O$ (Merck, $>98\%$), $NbCl_5$ (Merck, $>98\%$) as the precursors, acetylacetone (Merck, $>99\%$), and absolute ethanol (Merck, $>99\%$) as solvents. For this purpose, first $InCl_3$ was dissolved in acetylacetone and the resultant solution (0.2 M) was refluxed at 85 °C for 1 h. Then, the required amount of $SnCl_2.2 \cdot H_2O$ was dissolved in absolute ethanol at room temperature (0.2 M) and added as Sn dopant to the above solution. The resultant sol was mixed and refluxed at 85 °C for 1 h until transparent ITO sol was achieved. Then, the required amount of $NbCl_5$ was dissolved in absolute ethanol (0.2 M) and added to the ITO sol. These solutions were then mixed and refluxed at 85 °C for another 1 h until a transparent ITNO sol was achieved. Finally, the obtained sol was aged for 1 day at room temperature. Three different approaches for Nb-doping content in the ITO ($In_3Sn_4O_{12}$) thin films were considered: (I) For the first approach, In content was considered at 94 at% and Nb was added beside Sn dopant at a fixed 6 at% with general formula of $In_3Sn_{4-x}Nb_xO_{12}$ and atomic percent of Nb–Sn: 0.5–5.5 (S_1), 1–5 (S_2), 3–3 (S_3) and 5–1 (S_4). In this approach the main goal was to consider the substitution of the Sn with Nb in In_2O_3 lattice. (II) For the second approach, Nb was doped in ITO structure and its content was varied at 0.5 (S_5), 1 (S_6), and 3 at% (S_7) at a constant atomic ratio of In:Sn = 94:6 with general formula of $In_{3-x}Sn_{4-y}Nb_zO_{12}$ ($x+y=z$). In this approach Nb substitutes both In lattice sites and Sn. (III) For the third approach, Nb was added at 0.5 (S_8) and 1 at% (S_9) at a constant atomic ratio of In:Sn = 95:5 with general formula the same as Approach II. In this approach the main purpose was to consider the regions with higher In content than 94 at%. The composition and obtained electrical resistivity of the undoped ITO thin films (S_0) and these samples are summarized in Table 1.

2.2. Film preparation

The glass substrates were first washed with a detergent, next cleaned ultrasonically with deionized water and ethanol. Then, the prepared coating solution was deposited on the substrate by spin coating technique. Spin parameters, including spin speed and time, were fixed at 3000 rpm and 30 s, respectively. The coated substrates were dried at 200 °C after each step. Spinning and drying cycles were repeated in order to reach the desired film thickness. The films show a typical thickness of about 500 nm. Finally, the as-deposited films were annealed at a temperature of 500 °C in air atmosphere in electric furnace for 1 h. Fig. 1 shows the overall flow chart for ITNO thin films preparation via sol–gel spin coating technique.

2.3. Thin film characterization

The characteristics of nanostructured thin films were investigated by several analysis techniques. X-ray diffraction

Table 1
Composition and electrical resistivity of the prepared ITNO thin films.

Sample	Composition				Resistivity $\times 10^{-3}$
	In	Sn	Nb	Approach*	(Ω cm)
S_0	94	6	–	Reference sample	59.2
S_1	94	5.5	0.5	I	44.5
S_2	94	5	1	I	37.2
S_3	94	3	3	I	211.5
S_4	94	1	5	I	293.2
S_5	93.53	5.97	0.5	II	53.35
S_6	93.05	5.95	1	II	43.84
S_7	91.17	5.83	3	II	225.5
S_8	94.53	4.97	0.5	III	47.2
S_9	94.05	4.95	1	III	40.3

*(I) Nb–Sn dopant: fixed at 6 at% of total In, Sn, and Nb contents, (II) Nb added at fixed atomic ratio of In:Sn = 94:6, and (III) Nb added at fixed atomic ratio of In:Sn = 95:5.

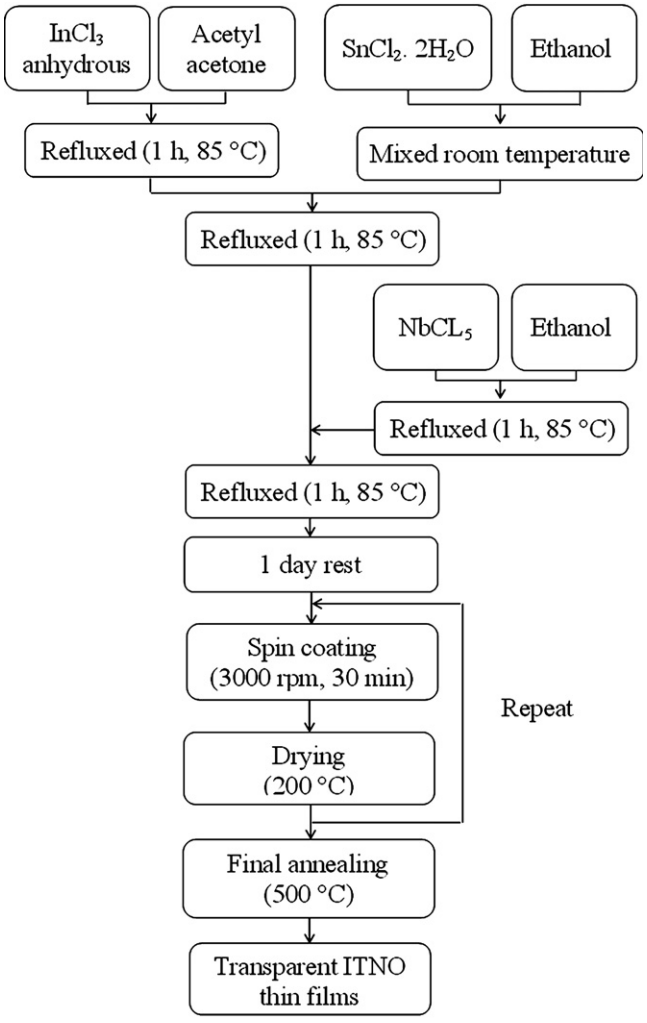

Fig. 1. A flow chart for ITNO thin films preparation.

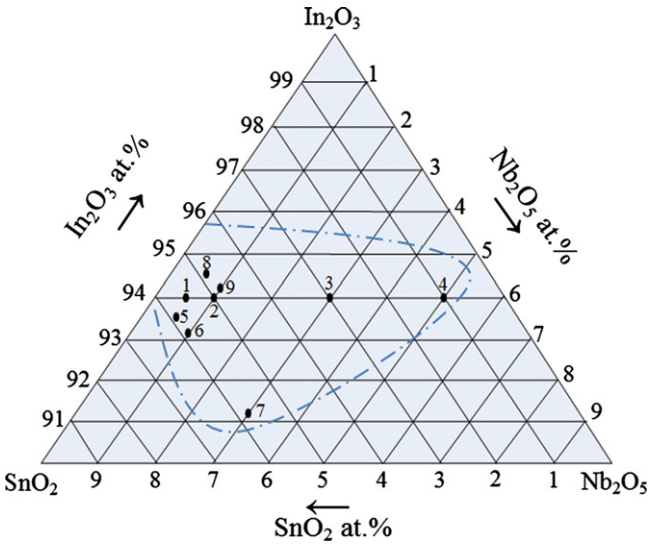

Fig. 2. In_2O_3–SnO_2–Nb_2O_5 partial triple diagram.

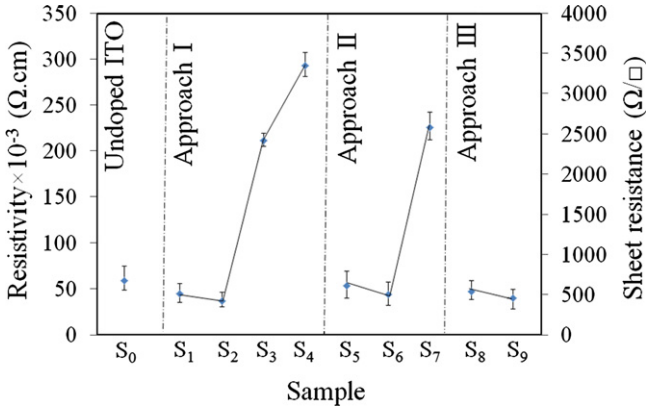

Fig. 3. Sheet resistance and electrical resistivity for undoped ITO (reference sample) and ITNO thin films according to the selected approach.

(XRD) patterns were obtained using an X-ray diffractometer, model Philips PW1730, with Cu K_α radiation ($\lambda = 1.5405$ Å, 40 kV, and 30 mA) in the range 29°–36° with step size of 0.02°. The mean particle size, morphologies, and surface roughness of the films were studied by field emission scanning electron microscopy (FESEM) model Hitachi S4160 and atomic force microscopy (AFM), model DME C26 operating in a non-contact mode. The resistivity of the films was measured by the four-point probe method Keithly model 196 Sys-DMM 2 at room temperature. The transmission spectra and optical band gap in the UV–vis–IR ranges (300–1000 nm wavelengths) were determined on a UV–vis Spectrophotometer PG instrument, model T80+.

3. Results and discussions

3.1. Electrical properties

As minimum electrical resistivity in In_2O_3 thin films was achieved at Sn-doping content of 6 at% [11,24], the first two approaches are based on the addition of Nb beside Sn dopant at fixed 6 at% or addition of Nb at constant atomic ratio of In:Sn = 94:6 in ITO structure. For the first approach, the prepared ITNO thin films (S_1–S_4 samples) can be located at positions 1–4 in the In_2O_3–SnO_2–Nb_2O_5 partial triple diagram in Fig. 2. The variation of sheet resistance and electrical resistivity of ITNO thin films according to the selected approaches are shown in Fig. 3. For comparison, the sheet resistance and electrical resistivity of undoped ITO film is included.

Approach I. For the first approach, the electrical resistivity of the films first decreases with increase in Nb-doping content, reaches a minimum resistivity of $37.2 \times 10^{-3}\ \Omega$ cm for composition S_2, and then increases with an increase in Nb-doping content so that resistivity of $293.2 \times 10^{-3}\ \Omega$ cm was obtained for composition S_4.

It was known that the Sn^{2+} ions transform to Sn^{4+} ions in an oxygen-rich environment [25]. Since all the samples

Table 2
Ionic radius, Lewis acid strength, and charge carrier difference of Nb^{5+}, Sn^{4+}, and In^{3+} ions.

Doping ions	Ionic radius (Å)	Lewis acid strength	Charge carrier difference with In^{3+}
Nb^{5+}	0.78	2.581	2
Sn^{4+}	0.71	0.228	1
In^{3+}	0.81	1.026	–

were annealed in air at 500 °C, the Sn ions exist in the form of Sn^{4+}. The initial decrease in electrical resistivity with increase in Nb-doping content until 1 at% can be related to two reasons. As In content was considered at a fixed content of 94 at%, there is a possibility that Nb^{5+} substitutes mostly Sn^{4+} instead of In^{3+}. As a result, substitution of Sn^{4+} ions with Nb^{5+} ions produce one free carrier per atomic substitution leading to an increase of carrier concentrations. Moreover, recent studies in chemical character of impurity dopant element in TCO materials revealed that the mobility of doped In_2O_3 thin films increases strongly with increase in the Lewis acid strength of the doping element [26]. The Lewis acid strength (L) can be calculated using a formula developed by Zhang [27] as

$$L = \frac{z}{r^2} - 7.7x_z + 0.8 \quad (1)$$

where r is the ionic radius related to the electrostatic force due to the oxidation state Z of the ion and x_z is the electronegativity of the element in the respective oxidation state. Ionic radius, Lewis acid strength, and charge carrier difference of Nb^{5+}, Sn^{4+}, and In^{3+} ions are summarized in Table 2. As can be seen, substitution of Sn^{4+} ions with Nb^{5+} ions increases both free carrier concentrations and mobility of Nb-doped thin films.

For higher Nb-doping contents, the resistivity increased due to the solubility limit of Nb atoms in In_2O_3 lattice in the sol–gel method. Moreover, increase of free carrier concentrations with the increase of Nb-doping content increases the electrical resistivity due to the increase of electron scattering and ionized impurity scattering. As a result, the minimum resistivity was achieved for the addition of Nb doping at the optimum content of 1 at% for composition S_2.

Approach II. For the second approach, the effect of Nb-doping content on the electrical properties of the ITO films was investigated through three different positions of 5–7 in the In_2O_3–SnO_2–Nb_2O_5 partial triple diagram with detailed compositions of In:Sn:Nb=93.53:5.97:0.5 (S_5), In:Sn:Nb=93.05:5.95:1 (S_6), and In:Sn:Nb =91.17:5.83:3 (S_7), respectively. In this approach electrical properties of ITNO thin films at 5 at% of Nb-doping content were not considered, due to maximum electrical resistivity, which was achieved at a content higher than the solubility limit of Nb in In_2O_3 matrix in the sol–gel process. The resistivity decreased from $59.2 \times 10^{-3}\,\Omega$ cm for undoped ITO films with the increase in Nb-doping content and reached a minimum of $43.8 \times 10^{-3}\,\Omega$ cm for Nb content of 1 at% for composition S_6. The reduction in electrical resistivity can be related to the incorporation of more Nb^{5+} into In_2O_3 lattice compared with Sn^{4+} as shown in the detailed composition of the prepared films. In fact, incorporation of Nb^{5+} ions with smaller ionic radii than In^{3+} causes less scattering and increase of free carrier concentration due to the valence difference between Nb^{5+} ions and In^{3+} ions. Also, improvement in conductivity can be related to increase of mobility due to the substitution of Nb^{5+} ions with higher Lewis acid strength than substituted In^{3+} lattice ions and also Sn^{4+}.

Further increase of Nb-doping content up to 3 at%, increases the electrical resistivity to $225.5 \times 10^{-3}\,\Omega$ cm. A probable reason is that the extra Nb atoms (more than 1 at%) do not occupy proper lattice positions in In_2O_3 matrix due to the solubility limit of Nb in presence of Sn. This results in increase of lattice distortion, electron scattering, and ionized impurity scattering, and thereby in increase of electrical resistivity.

Approach III. As can be observed, two previously considered approaches lead to the investigation of electrical properties of ITNO thin films at a fixed In content of 94 at% in the In_2O_3–SnO_2–Nb_2O_5 partial triple diagram and the contents lower than it. To investigate the regions which are rich with In contents, the effect of Nb-doping content at 0.5 and 1 at%, with minimum electrical resistivity in two previous approaches, was considered at a constant atomic ratio of In:Sn=95:5. The selected points can be located at positions 8 and 9 in the In_2O_3–SnO_2–Nb_2O_5 partial triple diagram with detailed composition of In:Sn:Nb =94.77:4.98:0.5 (S8) and In:Sn:Nb =94.05:4.95:1 (S9), respectively. In this approach, it can be noted that resistivity decreased from 47.2×10^{-3} to $40.3 \times 10^{-3}\,\Omega$ cm when Nb-doping content increased from 0.5 to 1 at% in the ITO lattice. Decrease of electrical resistivity for Nb-doping content up to 1 at% can be explained as substitution of Nb^{5+} ions into the In_2O_3 lattice and Sn^{4+}, which leads to increase of free carrier concentration, improvement of Lewis acid strength, and decrease of scattering centers and consequently improvement of conductivity and mobility. By considering detailed composition of prepared films in Approachs II and III (Table 1) at constant Nb-doping content (samples S_5 and S_8, S_6 and S_9) it can be seen that Approach III has less Sn dopant and more In than Approach II. Therefore, there is a higher possibility for substitution of Nb in In lattice sites than its substitution with Sn. According to the Table 2, there is less difference between ionic radii, more difference between Lewis acid strength, and also more difference between free carriers of Nb^{5+} and In^{3+} than those of between Sn^{4+} and In^{3+}; therefore, it is expected that less electron scattering, more mobility, and conductivity are achieved by substitution of Nb^{5+} with In-rich lattice sites. As a result, addition of Nb dopant in In-rich regions

(Approach III) is more beneficial than in regions with lower In content (Approach II).

With regard to the minimum resistivity achieved for ITNO thin films in three considered approaches (S_2, S_6, and S_9), the minimum electrical resistivity was achieved for addition of Nb-doping content at 1 at% in all of prepared ITNO thin films. Considering this point, it can be observed that the electrical resistivity decreased to lower values from the In_2O_3-based matrix (reference sample, S_0) to In:Sn:Nb=94.05:4.95:1 (Approach III, S_9), with addition of Nb in presence of Sn, and decreased more until minimum electrical resistivity was achieved for Nb–Sn doping contents of In:Sn:Nb=94:5:1 (Approach I, S_2). Salardenne et al. [28] reported similar observations for the ITGO (Sn+Ge-doped In_2O_3) thin films by adding Ge along with Sn in In_2O_3 thin films. Further increase of Sn content, In:Sn:Nb=93.05:5.95:1 (Approach II, S_6), increases the resistivity of ITNO thin films to higher degrees due to the increase in impurity scattering, and decrease of Lewis acid strength at higher Sn content compared with optimum Sn and Nb-doping contents of 5 and 1 at%.

Comparing three approaches shows that the minimum value of electrical resistivity obtained for S_2 in Approach I. This can be attributed to the substitution of Sn^{4+} ions with Nb^{5+} ions compared with substitution of Nb^{5+} ions with In lattice sites and Sn (Approachs II and III). As mentioned before, it is noteworthy to consider that lower Sn content is preferable due to its low Lewis acid strength and high difference between its ionic radius and In^{3+} ions which increases electron scattering. Therefore, substitution of Sn^{4+} with Nb^{5+} at constant In (sample S_2) in Approach I leads to increase of mobility and decreasing of scattering compared with Approachs II and III in which Nb^{5+} substitutes less Sn and more In lattice sites (sample S_6 and S_9).

As a result, the optimum electrical resistivity for ITNO thin films was achieved in Approach I. Therefore, the optical and microstructural properties of ITNO thin films were investigated in this approach with atomic percentages of Nb–Sn: 0.5–5.5, 1–5, 3–3, and 5–1 respectively.

3.2. Optical properties

The optical transmittance spectra of undoped ITO and ITNO thin films prepared for different Nb-doping contents of 0.5, 1, 3, and 5 at% in presence of Sn in the first approach is shown in Fig. 4. According to the this figure, the average optical transmittance of undoped ITO films increased with addition of Nb dopant, showing an average transmittance of about 85% in the visible region for ITNO films at Nb content of 1 at%. The increase in optical transmittance can be related to lower impurity scattering due to lower difference between ionic radii of Nb^{5+} ions and In^{3+} compared to the ones between Nb^{5+} and Sn^{4+} ions. On the other hand, the optical transmittance decreased to the average value of 65% with further increase of Nb-doping content to 5 at%, which could be due to the decrease in solubility limit of Nb in the In_2O_3 matrix; hence increase of lattice distortion as well as increase of electron scattering and ionized impurity scattering at higher carrier concentrations. In other words, increase in free carriers in higher Nb doping content leads to electron scattering and decrease in solubility of Nb in indium oxide lattice causes lattice distortion in some regions which greatly reduce the transparency.

Fig. 5 shows the variation of optical band gap for undoped ITO and ITNO films prepared with different Nb-doping contents of the first approach. The optical band gap (Eg) can be determined from the relation between absorption coefficient (α) and photon energy ($h\upsilon$) using Tauc's equation as follows [29]:

$$(\alpha h\upsilon)^2 = A(h\upsilon - Eg) \quad (2)$$

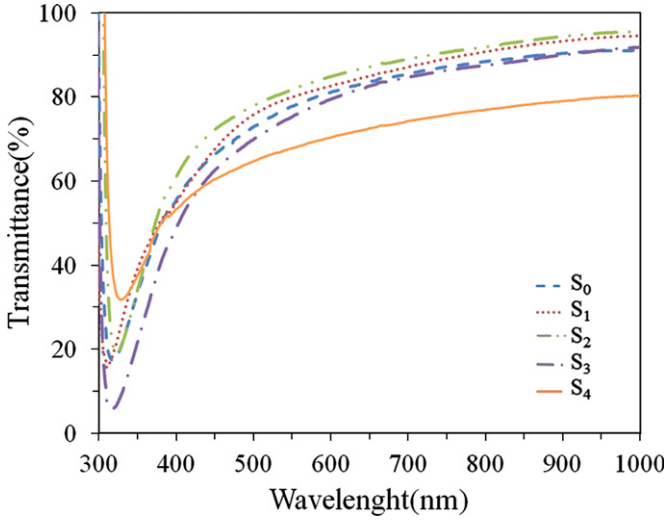

Fig. 4. UV–vis transmittance spectra of undoped ITO and ITNO thin films with different Nb-doping contents of first approach.

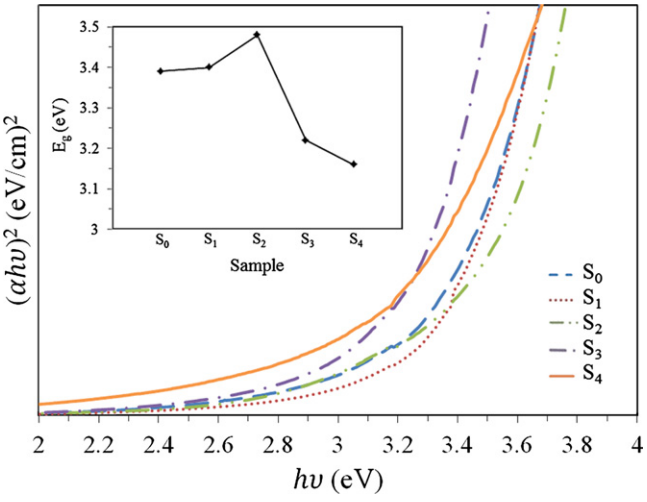

Fig. 5. The plot of $(\alpha h\upsilon)^2$ versus $h\upsilon$ for the undoped ITO and ITNO films with different Nb-doping contents of the first approach.

where $h\upsilon$, A and Eg are photon energy, constant, and optical band gap of the thin films, respectively. The optical band gap can be calculated from extrapolating the linear region of the $h\upsilon$-axis onto the energy axis. A value of 3.39 eV obtained for the undoped ITO films is found to increase to a range of 3.48 eV for Nb-doping content of 1 at%, after which it decreased to the value of 3.16 eV for Nb-doping content of 5 at%. Increase of band gap with addition of Nb-doping contents up to 1 at% can be explained as increase of free carriers due to the substitution of Nb^{5+} ions with Sn^{4+} ions, known as the Burnstein–Moss effect or blueshift [30]. At higher doping levels, increase in electron scattering, ionized impurity scattering, and lattice distortion as well as decrease in solubility limit of Nb in In_2O_3 matrix lead to the decrease of optical band gap, known as the band gap narrowing [31].

3.3. X-ray diffraction studies (XRD)

Fig. 6 shows the XRD patterns of ITNO films with different Nb-doping contents in the range of 0–5 at% in the first approach. It is observed that all of the peaks position in the XRD patterns are in a good agreement with the values given in JCPDS file no. 06-0416 for the cubic bixbyite structure of In_2O_3 [32] and JCPDS file no. 88–0773 for the rhombohedral structure of ITO [33], without any trace of other crystalline peaks, which indicates incorporation of Nb dopant besides Sn in the In_2O_3 lattice. As can be seen, the major peak position which is formed along the (222) plane shifted to lower diffraction angles with increase of Nb-doping content due to the difference between the ionic radii of Nb^{5+} ions and Sn^{4+} ions, which indicates increase in lattice constant. The lattice constant of undoped ITO film was determined to be $a=10.121$ Å, which increased to $a=10.182$ Å with increase in Nb dopant content. This shift in the peak position indicates incorporation of Nb in the In_2O_3 structure in the presence of Sn. Moreover, it was observed that the preferential orientation along (222) does not change to other peak position for Nb-doping content up to 5 at%.

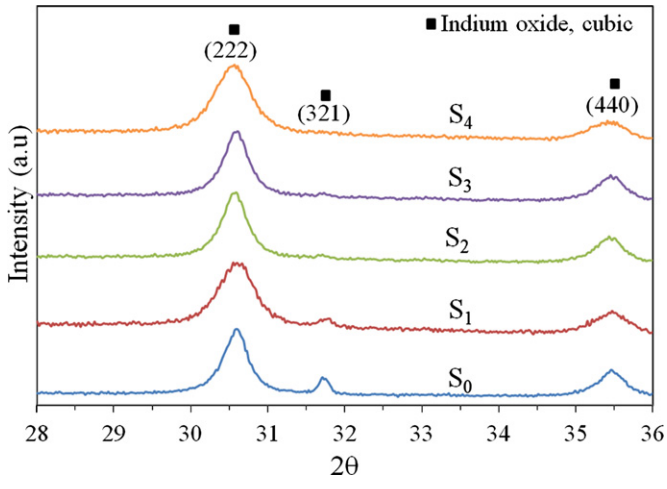

Fig. 6. XRD patterns of undoped ITO and ITNO films with Nb-Sn doping content of the first approach.

3.4. Microstructural studies

Fig. 7 shows the FESEM micrograph of the undoped ITO and ITNO films with different Nb-doping contents in the first approach. FESEM micrographs revealed the formation of nanostructured thin films with homogeneous and compact surface with nearly spherical and fine grained morphology. The average grain size of prepared films was found to be in the range 15–25 nm. It is well known that the average grain size reduces with increase of doping content. When impurities incorporated to lattice sites, they act as nucleation centers therefore nucleation rates increased. Moreover, addition of impurity increases interfacial energy; as a result further crystal growth is inhibited. Consequently, it is considerably more difficult for the doped crystal to grow compare to the pure host crystal in the absence of impurities [34]. However, in these samples the total amount of dopant is constant and the Sn was substituted with Nb and no trend in grain size with this substitution could be observed. Nevertheless, particle clustering occurs to reduce the interfacial energy which induced by decreasing of the particle size, as shown in Fig. 7c–e.

3.5. Surface morphology studies

Fig. 8 shows AFM images of the undoped ITO thin films with 6 at% of Sn dopant (reference sample, S_0) and Nb-doped ITO thin films with optimum opto-electronic properties at Nb–Sn atomic content of 1–5 (S_2), respectively. By analyzing the AFM images, the roughness of the films can be estimated through root mean square (RMS) roughness (S_q) and the average roughness (S_a) parameters. These parameters are important factors for opto-electronic devices since they directly affect the surface morphology of materials deposited on TCO electrodes.

AFM images indicate the formation of crystalline thin films with uniform and smooth surface for both films while the S_a and S_q parameters decreased by addition of Nb dopant beside Sn at an optimum content to In_2O_3 films from 10.23 to 4.82 nm and from 12.2 to 6.1 nm, respectively. Moreover, it is evident that lower surface roughness with more compact surface was achieved for ITNO films by addition of Nb doping besides Sn at the optimum content to the In_2O_3 lattice. The lower surface roughness could be attributed to the compact and homogenous Nb-doped films, as observed in the FESEM micrographs. The more compact surface of Nb-doped films attributed to fine-grained microstructure of the films. It is well known that more grain boundaries as a result of small particle size increases the scattering thereby decreases both conductivity and transparency of the films. However, more compact surface significantly decreases the average roughness and RMS factor of the films, which leads to TCOs with

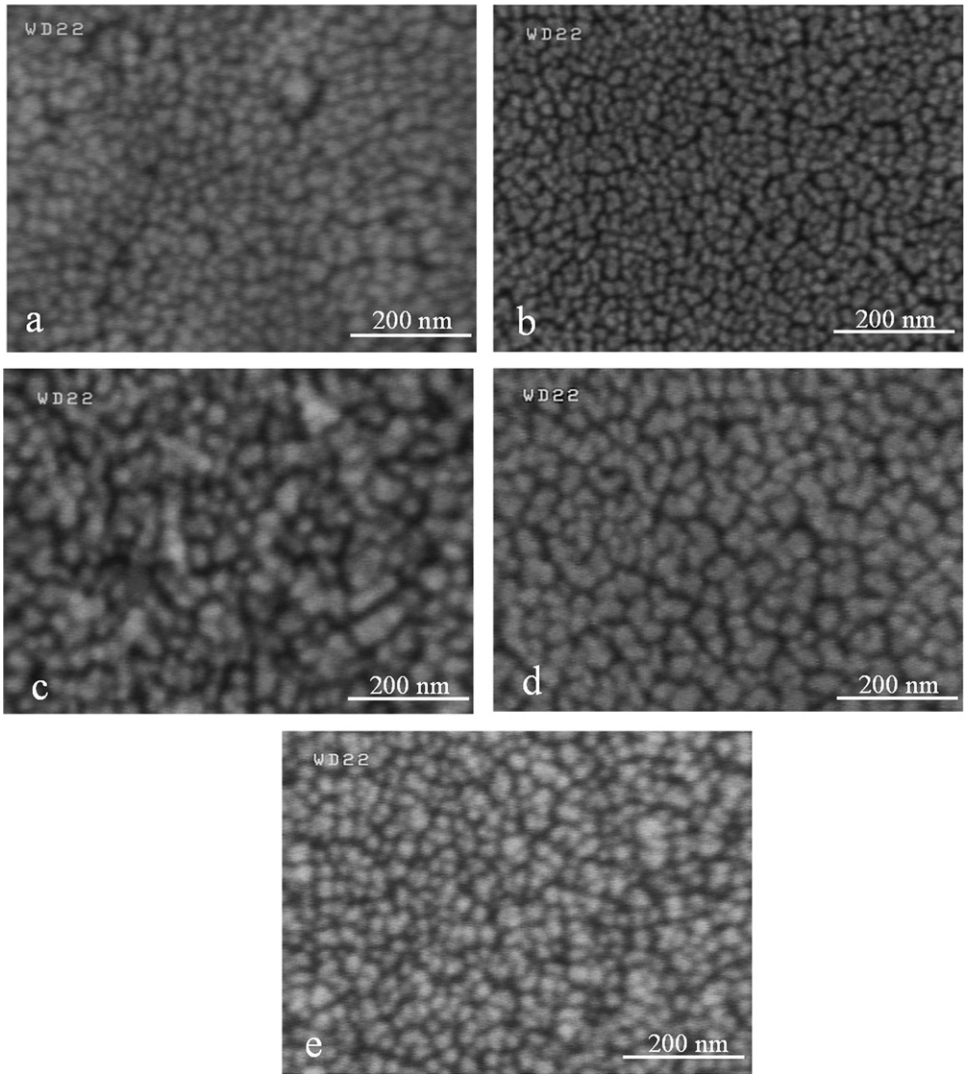

Fig. 7. FESEM micrographs of (a) undoped ITO thin films at 6 at% of Sn and ITNO thin films with Nb-doping contents of (b) 0.5, (c)1, (d) 3, and (e) 5 at% in the first approach.

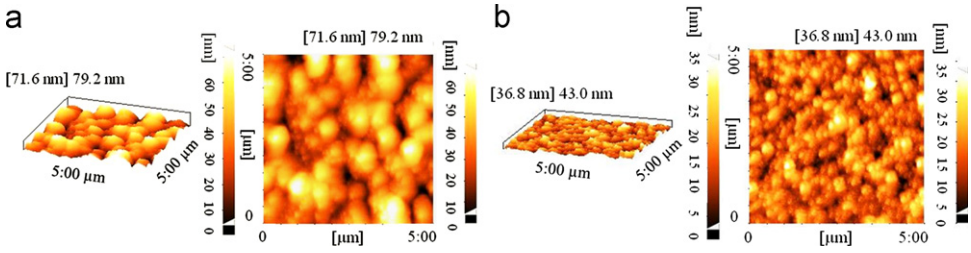

Fig. 8. Two-and three-dimensional AFM images for (a) undoped ITO (reference sample, S_0) and (b) Nb-doped ITO thin films with optimum opto-electronic properties (S_2).

better conductivity and higher transparency. It seems that the latter factor plays a key role in improving of opto-electronic properties of TCO films. As a result, the combination of more compact and homogenous surface with less average roughness provides new TCO with better opto-electronic properties compare to ITO films for applications in opto-electronic devices.

4. Conclusions

Nb-doped indium tin oxide (ITNO) nanostructured thin films with high optical transmittance and low resistivity have been synthesized successfully a via sol–gel spin coating technique for the first time. The influence of different Nb-doping contents on the electrical and optical as well as

microstructural properties of the films had been investigated systematically. The lowest electrical resistivity of $37.2 \times 10^{-3}\ \Omega$ cm and the average transmittance of about 85% in the visible region with a band gap of 3.48 eV was achieved for the ITNO films prepared with atomic content of Nb–Sn: 1–5 at fixed 6 at%. Improvement of opto-electronic properties compared to the undoped ITO films can be attributed to the substitution of Nb^{5+} ions with higher carrier concentration and Lewis acid strength compare to substituted Sn^{4+} ions, which leads to increase of free carriers and less impurity scattering at contents less than solubility limit of Nb-dopant in the In_2O_3 lattice. XRD studies show formation of thin films with similar patterns to In_2O_3 and ITO crystal structures for Nb-doped films, which represents a small shift in major peak position to lower values and increase in lattice constant due to incorporation of Nb beside Sn in the In_2O_3 structure. FESEM micrographs revealed that addition of Nb causes clustering of particles at higher doping content. AFM images show that surface quality parameters including average roughness and RMS roughness were reduced to lower values with addition of Nb at optimum content beside Sn to the In_2O_3 thin films.

References

[1] O.B. Regan, M. Gratzel, A low-cost high-efficiency solar cell based on dye sensitized colloidal TiO_2 films, Nature 353 (1991) 737–740.

[2] B.G. Lewis, D.C. Paine, Applications and processing of transparent conducting oxides, Materials Research Bulletin 25 (2000) 22–27.

[3] R.G. Gordon, Criteria for choosing transparent conductors, Materials Research Bulletin 25 (2000) 52–57.

[4] H. Kim, A. Pique, J.S. Horwitz, H. Mattoussi, H. Murata, Z.H. Kafafi, D.B. Chrisey, Indium tin oxide thin films for organic light-emitting devices, Applied Physics Letters 74 (1999) 3444–3446.

[5] Y.F. Sun, S.B. Liu, F.L. Meng, J.Y. Liu, Z. Jin, L.T. Kong, J.H. Liu, Metal oxide nanostructures and their gas sensing properties: a review, Sensors 12 (2012) 2610–2631.

[6] A. Beaurain, D. Luxembourg, C. Dufour, V. Koncar, B. Capoen, M. Bouazaoui, Effects of annealing temperature and heat-treatment duration on electrical properties of sol–gel derived indium–tin–oxide thin films, Thin Solid Films 516 (2008) 4102–4106.

[7] T.M. Hammad, Effect of annealing on electrical, structural and optical properties of sol–gel ITO thin films, Physica Status Solidi A 206 (2009) 2128–2132.

[8] H. Cho, Y.H. Yun, Characterization of indium tin oxide (ITO) thin films prepared by a sol–gel spin coating process, Ceramics International 37 (2011) 615–619.

[9] W.C. Chang, S.C. Lee, C.H. Yang, T.C. Lin, Opto-electronic prop-
erties of chromium doped indium–tin-oxide films deposited at room temperature, Materials Science and Engineering: B 153 (2008) 57–61.

[10] S. Kaleemulla, N.M. Rao, M.G. Joshi, A.S. Reddy, S. Uthanna, P.S. Reddy, Electrical and optical properties of In_2O_3: Mo thin films prepared at various Mo-doping level, Journal of Alloys and Compounds 504 (2010) 351–356.

[11] S. Seki, Y. Sawada, M.H. Wang, H. Lei, Y. Hoshi, T. Uchida, Electrical properties of tin-doped indium oxide thin films prepared by a dip coating, Ceramics International 38 (2012) S613–S616.

[12] L. Kong, J. Ma, F. Yang, C. Luan, Z. Zhu, Preparation and characterization of $Ga_{2x}In_{2(1-x)}O_3$ films deposited on ZrO_2 (100) substrates by MOCVD, Journal of Alloys and Compounds 499 (2010) 75–79.

[13] M. Sasaki, K. Yasui, S. Kohiki, H. Deguchi, S. Matsushima, M. Oku, T. Shishido, Cu doping effects on optical and magnetic properties of In2O3, Journal of Alloys and Compounds 334 (2002) 205–210.

[14] Y.C. Liang, Surface morphology and conductivity of zirconium-doped nanostructured indium oxide films with various crystallographic features, Ceramics International 36 (2010) 1743–1747.

[15] C. Lee, W. Lee, H. Kim, H.W. Kim, Influence of annealing atmosphere on the structure, resistivity and transmittance of InZnO thin films, Ceramics International 34 (2008) 1089–1092.

[16] K. Gupta, K. Ghosh, S.R. Mishra, P.K. Kahol, Opto-electrical properties of Ti-doped In_2O_3 thin films grown by pulsed laser deposition, Applied Surface Science 253 (2007) 9422–9425.

[17] R.K. Gupta, K. Gosh, S.R. Mishra, P.K. Kahol, High mobility W-doped In_2O_3 thin films: effect of growth temperature and oxygen pressure on structural, electrical and optical properties, Applied Surface Science 254 (2008) 1661–1665.

[18] Q. Zhang, X. Li, G. Li, Dependence of electrical and optical properties on thickness of tungsten-doped indium oxide thin films, Thin Solid Films 517 (2008) 613–616.

[19] S. Parthiban, V. Gokulakrishnan, K. Ramamurthi, E. Elangovan, R. Martins, E. Fortunato, R. Ganesan, High near-infrared transparent molybdenum-doped indium oxide thin films for nanocrystalline silicon solar cell applications, Solar Energy Materials and Solar Cells 93 (2009) 92–97.

[20] R.K. Gupta, K. Ghosh, S.R. Mishra, P.K. Kahol, Structural, optical and electrical characterization of highly conducting Mo-doped In_2O_3 thin films, Applied Surface Science 254 (2008) 4018–4023.

[21] R.K. Gupta, K. Ghosh, R. Patel, S.R. Mishra, P.K. Kahol, Effect of oxygen partial pressure on properties of Nb-doped In_2O_3 thin films, Materials Chemistry and Physics 112 (2008) 136–139.

[22] R.K. Gupta, K. Ghosh, R. Patel, P.K. Kahol, Effect of substrate temperature on opto-electrical properties of Nb-doped In_2O_3 thin films, Crystal Growth 310 (2008) 4336–4339.

[23] O. Lozano, Consequences of Nb-doping to ln_2O_3, a magneto–transport and optical study of a novel thin film transparent conductor, Ph.D. Thesis, University of Houston, USA, 2009.

[24] S. Seki, Y. Sawada, M. Ogawa, M. Yamamoto, Y. Kagota, A. Shida, M. Ide, Highly conducting indium–tin–oxide transparent films prepared by dip-coating with an indium carboxylate salt, Surface and Coatings Technology 169–170 (2003) 525–527.

[25] K. Dhananjay, C.W. Chu, C.W. Ou, M.C. Wu, Z.Y. Ho, K.C. Ho, S.W. Lee, Complementary inverter circuits based on p-SnO_2 and n-In_2O_3 thin film transistors, Applied Physics Letters 92 (2008) 232103–232105.

[26] S. Calnan, A.N. Tiwari, High mobility transparent conducting oxides for thin film solar cells, Thin Solid Films 518 (2010) 1839–1849.

[27] Y. Zhang, Electronegativities of elements in valence states and their appplications.1. Electronegativities of elements in valence states, Inorganic Chemistry 21 (1982) 3886–3889.

[28] J. Salardennea, C. Marcel, Y. Xu, G. Couturier, Electron scattering mechanisms in ITGO (Sn+Ge doped In_2O_3) thin films for low emittance window coatings, European Physical Journal 3 (1998) 233–235.

[29] J. Tauc, Amorphous and Liquid Semiconductors, Plenum Press, New York, 1974.

[30] S.M. Park, T. Ikegami, K. Ebihara, P.K. Shin, Structure and properties of transparent conductive doped ZnO films by pulsed laser deposition, Applied Surface Science 253 (2006) 1522–1527.

[31] A. Walsh, J.L.F. Da Silva, S.H. Wei, Origins of band-gap renormalization in degenerately doped semiconductors, Physical Review B 78 (2008) 75211–75215.

[32] Powder Diffraction File, JCPDS-International Centre for Diffraction Data—ICDD, Philadelphia, Card 06-0416, 1997.

[33] Powder Diffraction File, JCPDS-International Center for Diffraction Data, Philadelphia, Card no. 88–773, 1972.

[34] J.D. Bryan, D.R. Gamelin, Doped semiconductor nanocrystals: synthesis, characterization, physical properties and applications, Progress in Inorganic Chemistry 54 (2005) 47–126.